Effect of amphiphilic environment on the solution structure of mouse TSPO

translocator protein

Sophie COMBETa,*, Françoise BONNETEb,*, Stéphanie FINETc, Alexandre POZZAb, Christelle

SAADE^a, Anne MARTEL^d, Alexandros KOUTSIOUBAS^e, and Jean-Jacques LACAPERE^f

S. Combet and F. Bonneté are both 1st co-authors and *corresponding authors.

Email addresses: sophie.combet@cea.fr; francoise.bonnete@ibpc.fr

^aLaboratoire Léon-Brillouin (LLB), UMR12 CEA, CNRS, Université Paris-Saclay, F-91191 Gif-sur-

Yvette CEDEX, France. bUniversité Paris Cité, CNRS, Laboratoire de Biologie Physico-Chimique

des Protéines Membranaires (IBPC), F-75005 Paris, France. cInstitut de Minéralogie, de Physique de

Matériaux et de Cosmochimie (IMPMC), UMR 7590 CNRS, Sorbonne Université, MNHN, IRD, F-

75005 Paris, France. dInstitut Laue-Langevin (ILL), F-38042 Grenoble, France. Jülich Centre for

Neutron Science (JCNS) at Heinz Maier-Leibnitz Zentrum (MLZ), Forschungszentrum Jülich

GmbH, Lichtenbergstr. 1, D-85748 Garching, Germany. fLaboratoire des BioMolécules (LBM),

UMR 7203, Sorbonne Université, Ecole Normale Supérieure, PSL Université, CNRS, 4 place Jussieu,

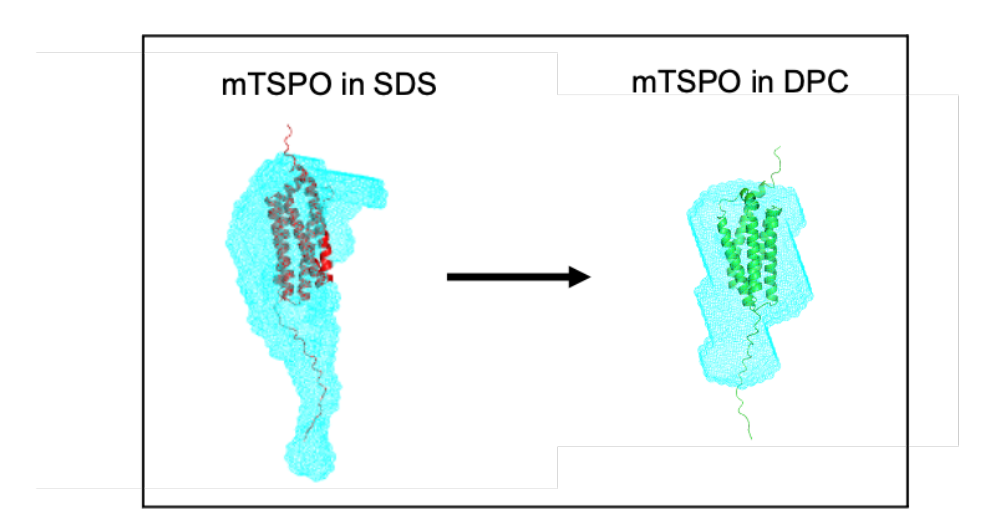
F-75005 Paris, France.

1

HIGHLIGHTS

- mTSPO 3D-structure is partially unfolded in SDS environment
- mTSPO can refold progressively to a more native state from SDS to DPC
- mTSPO helicity and coiled coil increase from SDS to DPC environment
- Intrinsic fluorescence from mTSPO 12 Trp increases in DPC compared to SDS
- mTSPO is more compact in DPC but not as much as in presence of a stabilizing ligand

GRAPHICAL ABSTRACT



KEYWORDS: membrane translocator mTSPO, SDS, DPC, MALLS, small-angle scattering (SAS), *ab initio* modeling.

ABBREVIATIONS: CD: circular dichroism; DM: decyl maltoside; DDM: dodecyl maltoside; DPC: dodecyl phosphocholine; MALLS: multi-angle laser light scattering; NMR: nuclear magnetic resonance; NSD: normalized spatial discrepancy; SANS: small-angle neutron scattering; SAXS: small-angle X-ray scattering; SEC: size-exclusion chromatography; SDS: sodium dodecyl sulfate; SLD (scattering length density); TSPO: translocator protein

ABSTRACT

The translocator protein (TSPO) is a ubiquitous transmembrane protein of great pharmacological interest thanks to its high affinity to many drug ligands. The only high-resolution 3D-structure known for mammalian TSPO was obtained by NMR for the mouse mTSPO in DPC detergent only in presence of the high-affinity PK 11195 ligand. An atomic structure of free-ligand mTSPO is still missing to better understand the interaction of ligands with mTSPO and their effects on the protein conformation.

Here, we decipher the solution structures of the recombinant mTSPO without ligand both in (i) SDS, the detergent used to extract and purify the protein from *E. coli* inclusion bodies, and (ii) DPC, the detergent used to solve the PK 11195-binding mTSPO NMR structure.

We report partially refolded and less flexible mTSPO helices in DPC compared to SDS. Besides, DPC stabilizes the tertiary structure of mTSPO, as shown by a higher intrinsic Trp fluorescence and changes in indole environment.

We evaluate by SEC-MALLS that ~135 SDS and ~100 DPC molecules are bound to mTSPO. SEC-small-angle X-ray (SAXS) and neutron (SANS) scattering confirm a larger mTSPO-detergent complex in SDS than in DPC. Using the contrast-matching technique in SEC-SANS, we demonstrate that mTSPO conformation is more compact and less flexible in DPC than in SDS. Combining *ab initio* modeling with SANS, we confirm that mTSPO conformation is less elongated in DPC than in SDS. However, the free-ligand mTSPO envelope in DPC is not as compact as the PK 11195-binding protein NMR structure, the ligand stiffening the protein.

1. INTRODUCTION

The translocator protein TSPO is a ubiquitous and functionally important membrane protein of about 18 kDa, present in different species from bacteria to plants, exhibiting a 5-helix transmembrane structure. In humans, the protein is found throughout the body [1]. In brain, TSPO is very little expressed in basal conditions but overexpressed with the neuroinflammation associated to many brain diseases [2]. TSPO has the capacity to bind multiple ligands which have been used as markers in neuroimaging [2]. Thus, multiple generations of positron emission tomography ligands for TSPO have already been synthesized [3]. The accessibility of the ligands to the protein binding cavities, as well as their stability inside, are crucial for drug design, whether for imaging, diagnostics, and therapies [3,4]. However, no atomic structure of the ligand-free mammalian TSPO is available so far [5,6]. Besides, the understanding of TSPO/ligand interaction remains unclear, as well as its effects on the protein structure. Solving such a structure still remains a challenge that would greatly facilitate the development of new molecules for medical applications.

Mouse TSPO (mTSPO from *Mus musculus*) folding strongly depends on its amphiphilic environment [5,7], leading to different affinity for its ligands [8,9]. Recombinant mTSPO is expressed in large amounts in *E. coli*, extracted and purified from inclusion bodies using the ionic sodium dodecyl sulfate detergent (SDS, Fig. S1, in Supplementary Information, SI) [8]. In SDS, the protein is in a stable and monodisperse monomeric form, but partially "unfolded", as previously shown by fluorescence, circular dichroism (CD), and liquid NMR [5]. Moreover, SDS-solubilized mTSPO is unable to bind any high affinity drug ligands, such as PK 11195 [9]. In contrast, mTSPO affinity in the zwitterionic dodecyl phosphocholine detergent (DPC, Fig. S1) is a few µM (*K*_{association}), as we measured previously [9], although lower than the nM affinity we observed in presence of lipids [8]. The exchange of SDS by DPC therefore allows mTSPO to recover a more "native" form, which made it possible to determine its high-resolution 3D-structure by liquid-state NMR (2MGY.PDB), the only one existing for a mammalian TSPO. However, this structure is described in presence of the specific PK 11195 ligand which stiffens the protein [10]. Indeed, in the same condition but without ligand,

mTSPO is very flexible [7] and several conformations coexist, as observed by intrinsic fluorescence, CD, and NMR [5,7]. Besides, all attempts to get crystals of mammalian TSPOs have failed so far, whereas two bacterial TSPOs were crystallized in lipid cubic phase from proteins purified in nonionic detergents (decyl or dodecyl maltoside, DM or DDM) from bacterial membrane [6,11]. In contrast, mTSPO is not stable in DM or DDM (JJ. Lacapère, personal communication). This might be due to a difference in the stability of mammalian and bacterial proteins solubilized in the detergents used to start protein crystallization or to the presence of co-purified lipids [12].

In order to decipher the influence of the amphiphilic environment on mTSPO structure, we combined light, X-ray, and neutron scattering with *ab initio* modeling to make a thorough biophysical characterization of mTSPO in solution in SDS or DPC detergents. The beneficial effect of DPC on SDS-purified mTSPO is shown first by changes in protein helicity, measured by circular dichroism (CD), confirmed by changes in its tertiary structure, from Trp intrinsic fluorescence and 1D 1H NMR data, and finally by size and 3D conformation changes by MALLS, SAXS, and SANS, as well as their interpretation with *ab initio* models.

We report that mTSPO solution structure is partially unfolded and flexible in SDS, whereas in DPC environment the protein recovers a more compact and structured conformation but still significantly different from the TSPO-PK 11195 described by NMR.

2. MATERIALS & METHODS

2.1. Detergent and buffer solutions

All salt and buffer reagents were purchased from Sigma or Anatrace. Sodium dodecyl sulfate (SDS) was obtained from Sigma (CAS number 151-21-3) and dodecyl phosphocholine (DPC) from Anatrace or CliniSciences (CAS number 29557-51-5). Deuterated sodium dodecyl-d25 sulfate (CAS number 110863-24-6) and dodecyl-d38-phosphocholine (CAS number 130890-78-7) were obtained from Cambridge Isotope Laboratories (USA). Heavy water (D₂O) was supplied by the Institut Laue-Langevin (ILL, France). In the following, "SDS/d-SDS" and "DPC/d-DPC" are used for the hydrogenated or deuterated forms of the detergents, respectively. Their structures are illustrated on Fig. S1 in SI. They are both used in all sample measurements at concentrations above the critical micelle concentration (CMC, Table S1).

2.2. mTSPO production and purification

Mouse TSPO (mTSPO) was expressed and purified as previously described [5,9,13]. Briefly, *E. coli* BL21 DE3, transfected with the pET15 plasmid containing mTSPO-cDNA (generous gift from Pr. V. Papadopoulos), were grown up in a LB medium and mTSPO was purified by polyhistidine-binding to Ni-NTA chelation resin (Qiagen, Les Ulis, France) in the presence of 2 mg/mL (0.2%) SDS (or d-SDS) in 50 mM HEPES, pH 6.8, 150 mM NaCl, and eluted with 300 mM imidazole. SDS was exchanged on the affinity column using 20 mg/mL (2%) DPC and mTSPO was purified with 2 mg/mL (0.2%) DPC (or d-DPC) before protein elution from the Ni-NTA column with 300 mM imidazole. The protein purity was analyzed by SDS-PAGE (12% acrylamide) run on a Protean II system (BioRad, Marnes-la-Coquette, France). The protein levels were quantified by UV spectra, using the absorption coefficient (3.88 mL.mg⁻¹.cm⁻¹ at 280 nm) calculated from the amino acid sequence composition.

2.3. Far UV circular dichroism experiments and analysis

Circular dichroism (CD) spectra were recorded on a ChirascanPlus spectropolarimeter (Applied Photophysics) from 180 to 300 nm in 2 mm pathlength Hellma cells, with 1 nm interval, and at 20°C. The mTSPO protein, purified in 2 mg/mL SDS in 50 mM HEPES, pH 7.8, 150 mM NaCl, 300 mM imidazole, was dialyzed against 10 mM phosphate buffer, pH 6.8, 2 mg/mL (0.2%) SDS to eliminate NaCl and imidazole. CD spectra were measured at the initial protein concentration of 5 μM (~0.1 mg/mL). DPC-induced changes were performed by adding increasing volume of concentrated DPC to the SDS-purified mTSPO sample.

Measurements were performed at 0.5 and 2 mg/mL (0.05 and 0.2%, respectively) DPC and then every 2 mg/mL (0.2%) until 20 mg/mL (2%) DPC. The DPC stock was prepared at 20% (200 mg/mL) in water, not in buffer. However, the volume addition to the pH-buffered samples during the titration was negligible compared to the sample volume (a few % of the total volume) and so no change in the sample pH was assumed. Blanks corresponding to micelles alone in the buffer were subtracted and the results were normalized to the protein concentration. The ratio of ellipticity measured at 222 and 208 nm ($\Delta \varepsilon_{222}/\Delta \varepsilon_{208}$) was used as an indicator of the presence of coiled-coils [14,15]. Subtracted and corrected spectra were smoothed and deconvoluted using BeStSel software (http://bestsel.elte.hu) to estimate the secondary structure content, especially the percentage of helicity [16]. The following titration equations were used to calculate, from the percentage of helicity or the $\frac{\Delta \varepsilon_{222 nm}}{\Delta \varepsilon_{208 nm}}$ ratio (both obtained directly from the CD measurements), the semi-saturation (SS) value of

% helicity =
$$\frac{[DPC]*(\%helicity)_{max}}{SS+[DPC]}$$
 Eq. 1

with (% helicity)_{max} the % of helicity at the DPC concentration needed to get a saturation (*i.e.* a plateau on the curve).

the titration curve:

$$\frac{\Delta \varepsilon_{222 nm}}{\Delta \varepsilon_{208 nm}} = \frac{[DPC]*(\frac{\Delta \varepsilon_{222 nm}}{\Delta \varepsilon_{208 nm}})_{max}}{SS+[DPC]}$$
 Eq. 1 bis

with $\left(\frac{\Delta \varepsilon_{222\ nm}}{\Delta \varepsilon_{208\ nm}}\right)_{max}$ the $\frac{\Delta \varepsilon_{222\ nm}}{\Delta \varepsilon_{208\ nm}}$ ratio at the DPC concentration needed to get a saturation (*i.e.* a plateau on the curve).

Results from four similar independent measurements were averaged with error evaluation. Fitting of the data was made using the Michaelis-Menten equation available in the Origin software (OriginLab).

2.4. Intrinsic Trp fluorescence experiments and analysis

Fluorescence measurements were carried out on a Cary Eclipse spectrofluorometer (Varian, France) at 20°C. Tryptophan fluorescence emission spectra were recorded at $\lambda = 335$ nm (*i.e.* the wavelength of the maximum intensity of emission fluorescence) in stirred 2 mL quartz Hellma cells between 300 and 450 nm (bandwidth of 2 nm, 0.5 nm steps), using an excitation wavelength of 290 nm (bandwidth of 2 nm). DPC-induced changes in intrinsic fluorescence spectra were performed by adding increasing volume of concentrated DPC to the 0.5 μ M protein (~0.01 mg/mL) SDS-purified mTSPO sample.

Measurements were performed every 0.1 mg/mL from 0 to 1 mg/mL (0.1%) DPC (from 20% DPC stock, see above), then every 0.5 mg/mL (0.05%) from 1 to 3 mg/mL (0.1 to 0.3%) DPC. Blanks, corresponding to the detergent alone in buffer, were subtracted from the respective spectra. Results from two similar independent measurements were averaged and normalized to the protein concentration by dividing the fluorescence intensity F for a given DPC concentration by the fluorescence intensity F_0 for [DPC] = 0, *i.e.* in SDS only as initially. The ratio $\frac{\Delta F}{F_0}$ was calculated, with $\Delta F = F - F_0$. The following titration equation, similar to Eqs. 1 and 1 bis, was used to calculate the semi-saturation (SS) value of the titration curve:

$$\frac{\Delta F}{F_0} = \frac{[DPC] * \left(\frac{\Delta F}{F_0}\right)_{max}}{SS + [DPC]}$$
 Eq. 2

with $\left(\frac{\Delta F}{F_0}\right)_{max}$ corresponding to $\frac{\Delta F}{F_0}$ ratio at the DPC concentration used to get a saturation (*i.e.* a plateau on the curve) and SS corresponding to the semi-saturation like in Eq. 1.

Results from three similar independent measurements were averaged with error evaluation. Fitting of the data was made using the Michaelis-Menten equation available in the Origin software (OriginLab).

2.5. 1D 1H NMR experiments and analysis

NMR measurements were carried out on a Bruker 500 MHz spectrometer equipped with a cryogenic triple resonance probe at 25°C. DPC-induced changes in 1D 1H spectra were recorded with a sample containing 0.1 mM mTSPO (~2 mg/mL) in 10 mM phosphate buffer (pH 6.5) H₂O:D₂O (9:1) solution containing 2 mg/mL (0.2%) SDS by adding increasing volume of concentrated (20% stock, see above) DPC to get the final concentrations of 4, 6, 8, and 10 mg/mL (from 0.4 to 1%) of DPC in the samples. The following titration equation, similar to Eqs. 1, 1 bis, and 2, was used to calculate the semi-saturation (SS) value of the titration curve:

$$Cs_{Indole} = \frac{[DPC]*(\Delta Cs)_{max}}{SS+[DPC]}$$
 Eq. 3

with $(\Delta Cs)_{max}$ corresponding to the chemical shift (Cs) for the indole at the DPC concentration used to get a plateau minus the Cs in the absence of DPC (*i.e.* in presence of SDS only as initially) and SS corresponding to the semi-saturation.

2.6. SEC-MALLS experiments and analysis

The absolute mass determination (*i.e.* without column calibration with MW standards) of mTSPO-detergent complexes, detergent moiety around mTSPO, and protein oligomeric states in the two detergents were carried out by size-exclusion chromatography (SEC) coupled to multi-angle laser light scattering (MALLS) on a Shimadzu HPLC coupled to an Optilab® T-rEXTM refractometer and a miniDawnTM TREOS detector (Wyatt Technology). Two SEC columns, compatible with the Shimadzu LC-20AD pump, and allowing suitable conditions to separate the protein-detergent complexes from free micelles (detergent micelles in absence of mTSPO), were used: (*i*) Agilent Bio Sec-3 (4.6/300, 5 mL) for mTSPO-SDS and (*ii*) Cytiva Superdex Increase 75 (10/300, 24 mL) for mTSPO-DPC. The mTSPO-SDS complex being larger than SDS micelles, they were both well separated on an Agilent BioSec-3 column, in contrast with mTSPO-DPC complex and DPC micelles

(Fig. S2, A-B). A Superdex S75i column, which is more resolutive for mTSPO-DPC complex, was therefore needed (Fig. S2C).

Absolute molar masses (MM) of each macromolecule (i.e. protein-detergent complexes and free detergent micelles) passing through the column were determined, by measuring simultaneously the static light scattering signal at three angles (44, 90, and 136°), knowing both protein and detergent concentrations from the extinction coefficient ($\varepsilon_{0.1\%}$ at 280 nm) and the refractive index increment $(\partial n/\partial c)$. For mTSPO protein, the extinction coefficient at 0.1% protein concentration (1 mg/mL), noted $\varepsilon_{0.1\%}$, is equal to 3.88 mL.mg⁻¹.cm⁻¹ at 280 nm and $\partial n/\partial c$ is found equal to 0.197 mL.g⁻¹ from SedFit software. For the two detergents, $\varepsilon_{0.1\%} \approx 0$ at 280 nm and $\partial n/\partial c$ was measured in 50 mM HEPES, pH 7.8, 150 mM NaCl using the Optilab® T-rEXTM refractometer and found equal to 0.1195 mL.g-1 and 0.1214 mL.g-1 for SDS and DPC, respectively. Mass fractions of mTSPO and bound detergent were calculated using the automatic procedure "Protein Conjugate" in the software Astra V (see [17] for more details). A volume of 20 μL of mTSPO-SDS at 10 mg/mL (i.e. 200 μg complex) and mTSPO-DPC at 5 mg/mL (i.e. 100 µg complex) were injected onto the Agilent BioSec-3 column for SDS and onto the Cytiva Superdex S75i for DPC. The samples were eluted with 50 mM HEPES buffer, pH 7.8, 150 mM NaCl, and 1 mg/mL detergent (i.e. 0.1 % SDS or DPC) at a flow rate of 400 μL/min and a temperature of 20°C. Mobile phases contain detergents above their CMC to avoid demicellization of the protein belt and free micelles in the samples, which could induce mTSPO aggregation.

2.7. SEC-SAXS experiments and analysis

SEC-SAXS experiments were performed on SWING beamline at the French synchrotron facility SOLEIL (St-Aubin, France) [18], using a wavelength of $\lambda = 1.03$ Å and a sample-to-detector distance of 2 m. The achievable q-range was 0.0045 to 0.546 Å-1, where $q = \frac{4\pi}{\lambda} sin\theta$ is the momentum transfer and 2θ the scattering angle. In order to determine an "ideal" form factor of mTSPO-detergent complex (*i.e.* without interference of weak interactions, therefore without structure

factor), in both SDS and DPC, three sample volumes (*i.e.* 3 amounts of about 100-125, 250, and 500 μg) of mTSPO-detergent complex were injected onto the same SEC columns, as used for SEC-MALLS, with 50 mM HEPES buffer, pH 7.8, 150 mM NaCl and 0.1% (1 mg/mL) detergent (SDS or DPC) at a flow rate of 300 μL/min and a temperature of 20°C, using the Agilent HPLC system online with the SAXS flow cell. The protein concentration was measured at 280 nm in the HPLC UV-vis cell. SAXS images were collected during the SEC elution, with a frame duration depending on the volume of the column: 990 msec for the 5 mL column and 4 sec for the 24 mL column. The 2D-SAXS patterns were normalized to the transmitted intensity and azimuthally averaged using the Foxtrot program (Java-based graphical application developed at SOLEIL and available at http://www.synchrotron-soleil.fr/Recherche/LignesLumiere/SWING).

Both forward intensity I(0) and radius of gyration (R_G) were determined using the Guinier approximation $I(q) = I(0).\exp(-(qR_G)^2/3)$, in the domain $q.R_G < 1.3$, and a scattergraph (i.e. a double Y-axis graph, I(0) and R_G) was plotted as a function of frame (Fig. S3, A-B) [19]. For each injected volume, SAXS curves were selected in a stable range of $R_{\rm G}$, subtracted for buffer and averaged. The three volumes of mTSPO-detergent injected on the column allowed to evaluate possible weak interactions between mTSPO-detergent complexes and to build an "ideal" form factor (i.e. the intramolecular correlations that allow to access in our conditions to the protein conformation) [19] for ab initio modeling. Indeed, the two detergents, SDS and DPC, are ionic detergents that may present repulsive interactions depending on the solvent conditions (pH, salt ionic strength). The "ideal" form factors of mTSPO-SDS and mTSPO-DPC were thus obtained by merging the low q-range SAXS curve, where interactions are negligible, with the large q-range SAXS curve at high concentration, where the signal is less noisy, after verifying that the concentration-normalized SAXS curves are superimposed at large q (Fig. S3, C-D). Resulting SAXS form factors were then analyzed in terms of pair-distance distribution function (P(r)) to obtain the "real space" R_G and the maximum distance within the complex (D_{max}) using the indirect Fourier transform method (GNOM) from the ATSAS package [20] (Fig. S3, E-F). A Kratky analysis (i.e. using $q^2I(q)$ as function of q, that allows

to evaluate if a macromolecule is compact, flexible, or unfolded [21]) was performed to assess the degree of unfolding state of the complex in the two detergents [22]. The R_G -dimensionless Kratky plot is the same representation but using $(qR_G)^2I(q)$ as function of qR_G [23]. In such a representation, a globular 3D-structure is highlighted by a bell-shape and a first maximum value of 1.1 at $q.R_G \approx \sqrt{3}$ [24]. All SAXS analysis were performed by using BioXTAS RAW, an open-source software [25].

2.8. SEC-SANS experiments and analysis

Small-angle neutron scattering (SANS) experiments were performed on D22 diffractometer (ILL, Grenoble, France). Two configurations were used for experiment in SDS: a 6 Å wavelength and sample-detector distances of 2 m (off-centered by 300 mm to get a larger *q*-range) and 5.6 m. For experiment in DPC, only one sample-detector (5.6 m) was necessary since an additional front detector was installed in the instrument. As for SEC-SAXS, we used a SEC column compatible with the HPLC pump of D22 and the SANS Hellma cell volume, *i.e.* a Superdex 200 HR (10/300, 24 mL) [26]. We measured mTSPO-detergent complexes using hydrogenated or deuterated detergents in 50 mM HEPES, 150 mM NaCl, pD 6.6, with different H₂O:D₂O ratios in the three following contrast conditions: (*i*) mTSPO/h-detergent in 100% D₂O solvent to measure the whole protein-detergent complex; (*iii*) mTSPO/d-detergent in 42% D₂O solvent to contrast-match the hydrogenous protein and measure the detergent belt only; (*iiii*) mTSPO/d-detergent in 100% D₂O solvent to contrast-match the deuterated detergent and measure the protein only. We checked experimentally that, in 100% D₂O buffer, d-SDS and a mixture of 86% d-DPC/14% h-DPC are fully contrast-matched (not shown).

Guinier analysis was done using the NIST SANS data analysis program (https://www.nist.gov/ncnr/data-reduction-analysis/sans-software) and parameters in the real space were calculated from GNOM (ATSAS package [20]).

2.9. Ab initio modeling and AlphaFold prediction

Ab initio modeling of the detergent belts was performed from SAXS curves, using MemProt software [27] with, either 2MGY.PDB structure of mTSPO-PK 11195 in DPC from NMR, or the best AlphaFold model from His-tagged mTSPO without ligand. The principle of the MemProt method is detailed in the SI (p. 8) and in Berthaud *et al.* [28].

Ab initio reconstructions of mTSPO were performed from the SANS curves in the condition where the detergent was contrast-matched, using the DENFERT program [29,30]. This software is based on Monte Carlo calculations to reconstruct a low-resolution shape from SAS scattering data, taking into account the hydration layer contribution to the scattering (see DENFERT WebServer: https://alexandros-koutsioumpas.github.io/Denfert/). The modeling was repeated 10 times and the normalized spatial discrepancy (NSD) values between all 10 models was calculated using the DAMSUP/SUPCOMB programs from ATSAS [31]. The model with the best score was then aligned and compared with an all-atom structure.

Five models of mTSPO were calculated using AlphaFold (AI system developed by DeepMind [32,33]) from the His-tagged mTSPO sequence (P. Legrand, personal communication). The most precise one (*i.e.* with the best rank) was compared to the only available NMR model from mTSPO-PK 11195 in DPC (2MGY.PDB) (Fig. S4). As the superimposition shows a good matching of most of the protein helices, the AlphaFold model was used with confidence to compare with the envelopes modeled from the experimental SANS data. Both models were compared, but the AlphaFold model was *a priori* preferred to the 2MGY.PDB NMR model because, unlike the latter, the AlphaFold model takes into account both the His-tag and the apo form (without the PK 11195 ligand) of the protein, as in the present study.

3. RESULTS & DISCUSSION

3.1. Ellipticity of mTSPO-detergent complex

Addition of DPC to SDS-purified mTSPO induces a large change in the CD spectra (Fig. 1A), as previously described [5], with an increase in the maximum around 190 nm and a decrease around 210-220 nm, which is characteristic of an increase in α -helix content. Deconvolution of CD spectra show, with increasing concentrations of DPC, an increased helical content from ~28% (mTSPO in SDS only) to ~37% (mTSPO in DPC only, at the saturation), a semi-saturation (SS) value of ~0.09 mg/mL DPC, and a saturating DPC concentration at ~3-4 mg/mL (Fig. 1B). The increase in $\Delta\epsilon_{222}/\Delta\epsilon_{208}$ ratio (Fig. 1C) suggests a different protein structuration with an increase in inter-helical interactions [14,15] in DPC compared to SDS, that could explain why mTSPO is able to bind high affinity ligands in DPC but not in SDS [5]. SS value for $\Delta\epsilon_{222}/\Delta\epsilon_{208}$ ratio is of ~0.03 mg/mL DPC with a saturating DPC concentration at ~3 mg/mL (Fig. 1C), comparable to the result for helicity content (Fig. 1B).

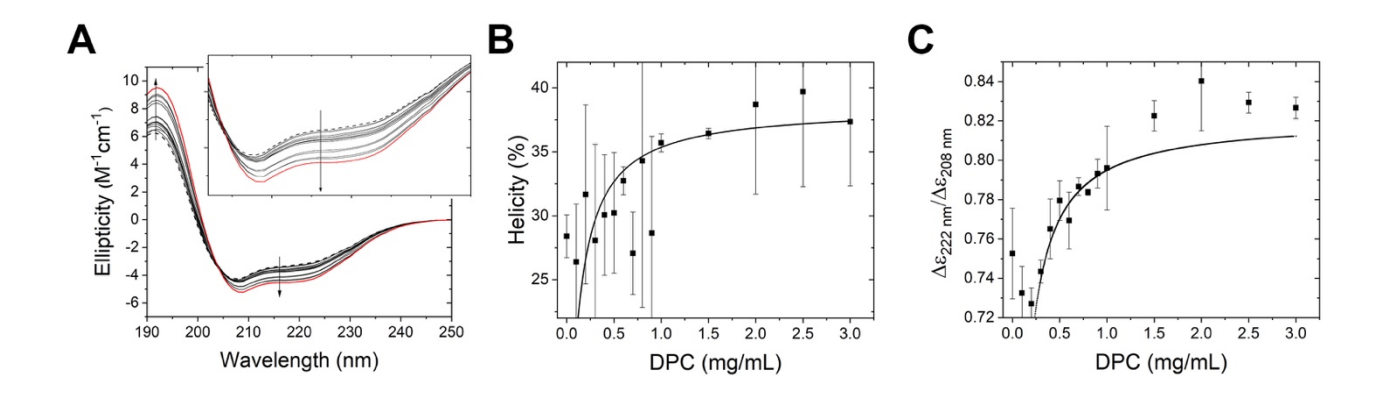


Figure 1. Changes in mTSPO secondary structure induced by DPC addition to the protein. (*A*) CD spectra of mTSPO in 20 mg/mL (2%) SDS (initial protein concentration of 5 μM) (black dash line) and upon further addition of DPC: every 0.1 mg/mL from 0.1 to 1 mg/mL, then at 1.5, 2, 2.5 (black lines), and finally at 3 mg/mL (0.3%, red line) (see insert for details). (*B*) Helix content of mTSPO as function of the DPC added to the buffer. Individual spectrum for each condition was treated with BeStStel software to get the percentage of helicity. (*C*) Evolution of $\Delta \epsilon_{2222 \text{ nm}}/\Delta \epsilon_{208 \text{ nm}}$ ratio as function

of the DPC added to the buffer. Saturation curves (lines) fitting the experimental data are drawn using Eqs 1 and 1 bis in (\mathbf{B}) and (\mathbf{C}), respectively ($\chi^2 = 0.77$ and $\chi^2 = 5.87$, respectively).

3.2. Trp intrinsic fluorescence of mTSPO-detergent complex

The addition of increasing DPC concentrations to mTSPO purified in 2 mg/mL (0.2%) SDS induces an increase in the emission spectrum of mTSPO intrinsic fluorescence (Fig. 2A), as previously reported [5,9]. This large increase suggests a change in the 12 mTSPO Trp environment, in agreement with the helical refolding observed by CD. However, the titration by fluorescence reveals a significant difference in concentration dependence compared to CD. A much higher DPC concentration (~15 mg/mL) is needed to get the fluorescence saturation (plateau) (Fig. 2B) compared to CD titration (~4 mg/mL DPC, Fig. 1, B-C). This result is in agreement with the much higher SS value found (~3.5 mg/mL) in fluorescence compared to CD (less than 0.1 mg/mL). This suggests that the secondary structure refolding (*i.e.* inter-helical interaction and helix content) may take place before side chain Trp environment changes.

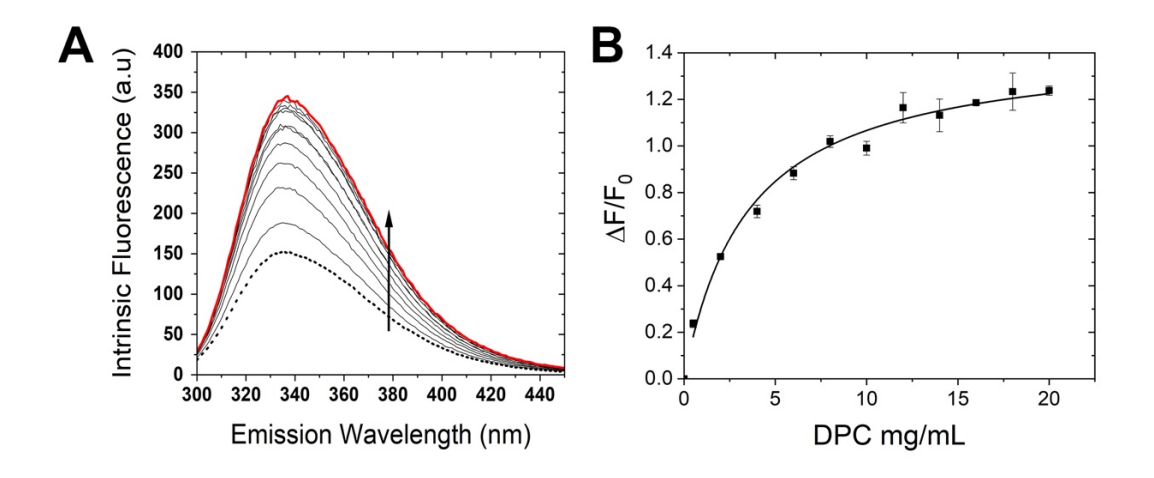


Figure 2. Changes in intrinsic Trp fluorescence spectra of mTSPO in 2% (20 mg/mL) SDS (initial protein concentration of 0.5 μM) induced by DPC addition. (*A*) Fluorescence Trp emission spectra of SDS-purified mTSPO (black dash line) with an excitation wavelength of 290 nm and upon further addition of increasing concentration of DPC: 0.5, 2, 4, 6, 8, 10, 12, 14, 16, 18 mg/mL (black lines),

and finally 20 mg/mL (2%, red line). (**B**) Corresponding relative intrinsic fluorescence changes of mTSPO, as function of DPC concentration, modeled with the titration Eq. 2 (line, $\chi^2 = 2.7$).

3.3. Indole content in mTSPO-detergent complexes

To further study the effect of DPC on Trp environment, we recorded 1D 1H NMR spectra of mTSPO purified in 2 mg/mL SDS at increasing DPC concentrations, focusing on the indole region corresponding to Trp residues (Fig. 3A). DPC addition induces both an increase in the intensity of the massif and a chemical shift (Cs) of the indole peak (Fig. 2A). Titration curve, obtained from NMR data (Fig. 3B), is in agreement with fluorescence titration observed upon DPC addition (Fig. 2B), with a similar DPC concentration to get the plateau (~14 mg/mL), as well as SS value (~4 mg/mL). The presence of a small indole massif in SDS condition, instead of sharp peaks, suggests that each of the 12 Trp residues in mTSPO has not a single orientation. The addition of DPC modifies the indole region, leading to the appearance of a sharper peak, with a shoulder and a smaller peak. This suggests the reorganization of several Trp in a more homogeneous form, in agreement with the increase in fluorescence intensity as shown in Fig. 1A. However, 1D 1H spectra do not permit to distinguish the 12 Trp as previously described in the literature [5,7].

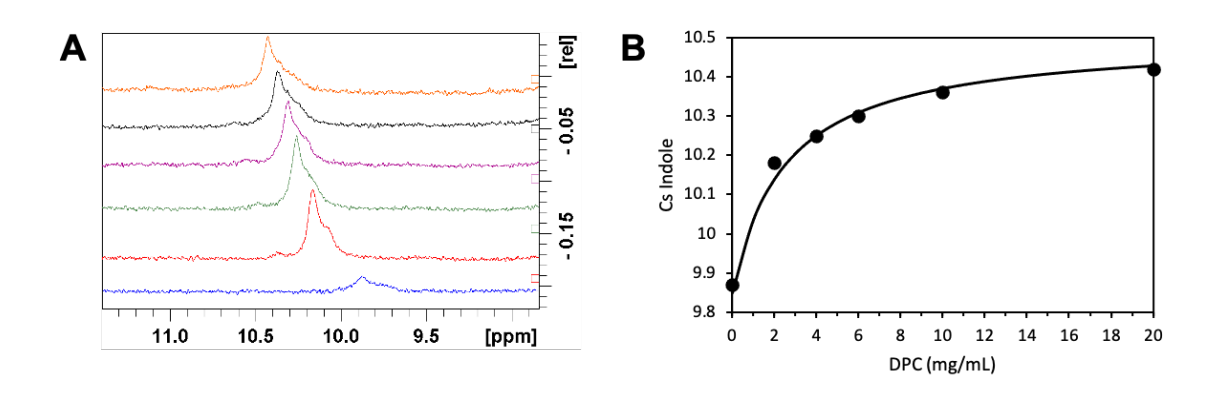


Figure 3. Changes in 1D 1H spectra of mTSPO induced by DPC addition to the protein purified in SDS (2 mg/mL). (*A*) Individual spectrum in the indole region of mTSPO (300 μM) purified in SDS (blue line) and upon further addition of 2, 4, 6, 8, and 10 mg/mL of DPC (red, green, purple, black,

and orange lines, respectively). (*B*) Chemical shift (Cs) of the maximum of the indole massif of mTSPO as a function of DPC addition in the medium, modeled with Eq. 3 titration (line).

According to these results, we purified mTSPO in DPC by exchanging SDS directly on the Ni-NTA affinity column by 20 mg/mL (2%) DPC, followed by elution with 2 mg/mL (0.2%) DPC. We then compared the structures in solution of both mTSPO-SDS and mTSPO-DPC complexes by scattering techniques, using light scattering to determine the oligomeric state of mTSPO and the amount of bound detergents, SAXS to describe the shape of the whole complexes, and SANS to describe, with *ab initio* modeling, the shape of the protein alone, the detergent being matched-out.

3.4. Characterization of mTSPO-detergent complexes by SEC-MALLS

Before studying the solution structures of membrane protein-detergent complexes by small-angle scattering (SAXS or SANS) techniques, it is essential to check by SEC-MALLS the homogeneity of the complex and to determine the suitable physico-chemical conditions (type of column, mobile phase, pH, salts, ionic strength) in which the protein-detergent complex is well separated from both extra free detergent micelles and void-volume aggregates. Indeed, SEC-MALLS allows to characterize the monodispersity of the complexes and the oligomeric state of mTSPO and to determine the number of detergent molecules ($N_{\rm det}$) bound to mTSPO by calculating the molar mass of each component.

The UV-chromatogram (Fig. S2A) shows that mTSPO-SDS complex elutes well separated from free SDS micelles that elute at a higher volume (V = 4 mL) and far from the void volume ($V_0 = 2 \text{ mL}$). The mTSPO-SDS complex is monodisperse (Fig. 4A) (*i.e.* the calculated molar mass (MM) depicts as a horizontal line) in the elution peak of SEC-MALLS, which is suitable for further SAS experiments. mTSPO-SDS appears as a monomer of about 19 kDa, which is rather in agreement with the theoretical mass of the recombinant His₆-tagged protein (\sim 21 kDa), calculated from mTSPO sequence (\sim 18 kDa) and the addition of the His₆-tag. Due to repulsive interactions between mTSPO-

SDS complexes, as observed from SAXS data (Fig. S3C), the molar mass of the complex is underestimated, *i.e.* the mass of both mTSPO and its bound SDS belt. The calculated number of detergent molecules bound to mTSPO is about 135 SDS molecules (Table 1).

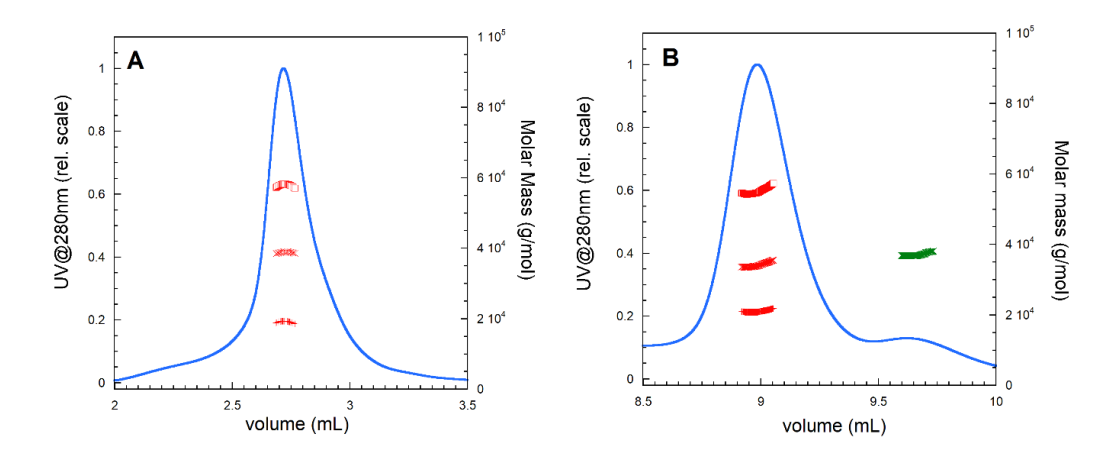


Figure 4. SEC-MALLS analysis of mTSPO-SDS (A) and mTSPO-DPC (B) complexes. Blue lines represent the UV signal at 280 nm. Molar masses (MM) are calculated and depicted for both mTSPO-detergent complexes (\square): mTSPO protein (+), its bound detergents (\times), and the free DPC micelles (\times). The SDS free micelles are not visible in this elution condition.

mTSPO-DPC complex and free DPC micelles being not separated enough on the column used with mTSPO-SDS (Fig. S2B), a longer and more resolutive column was chosen (Fig. S2C). Fig. 4B depicts both the UV signal at 280 nm during the elution of mTSPO-DPC complex through the Superdex 75 Increase (10 x 300) column and the calculated molar masses of mTSPO in DPC and bound-DPC around TSPO, as well as of free DPC micelles. The free DPC micelles elution (V = 10 mL) is well-separated from TSPO complex (V = 9 mL) enabling a more accurate calculation of mTSPO MM consistent with a monomeric form (Table 1). In DPC, the molar mass of mTSPO is about 21 kDa, identical to the calculated molar mass of the His₆-tagged TSPO. The number of DPC molecules bound to the transmembrane domain is about 98 molecules, lower than the 135 SDS molecules (Table 1). Although SDS and DPC have the same hydrophobic chain length, more SDS than DPC molecules bind to mTSPO. This can be due, either to a larger detergent belt around mTSPO

in SDS compared to DPC, or to a more unfolded structure of mTSPO in SDS than in DPC, allowing a larger surface of detergent interaction, or both.

3.5. Characterization of mTSPO-detergent complex by SEC-SAXS

3.5.1. Characterization of mTSPO-detergent whole complex

From the SAXS curves of mTSPO-SDS, corresponding to the three injected volumes (Fig S3, A & C) repulsive interactions between complexes are observed (both the apparent R_G in Fig. S3A and the forward intensities I(0) in Fig. S3C decrease as injected amount of mTSPO-SDS increases), while the form factor of the mTSPO-SDS complex remains unchanged (the three concentration-normalized curves superimpose for $q > 0.05 \text{ Å}^{-1}$). From the Guinier plot (Fig. 5A, insert), we found a mTSPO-SDS complex R_G of 37.4 Å and, from pair-distance distribution function P(r) (Fig. 5B) a D_{max} (*i.e.* the maximum distance within the complex) of 115 Å. These values are much larger than the theoretical R_G calculated, either from 2MGY.PDB, the atomic structure of mTSPO-PK 11195 in DPC ($R_G = 18 \text{ Å}$, $D_{max} = 67 \text{ Å}$), or AlphaFold model from His-tagged mTSPO ($R_G = 21 \text{ Å}$), suggesting a large SDS belt around mTSPO. The dimensionless Kratky plot (Fig. 5C) shows that mTSPO-SDS complex presents a globular shape, as highlighted by the first maximum at $q.R_G = \sqrt{3} \approx 1.73$ [24].

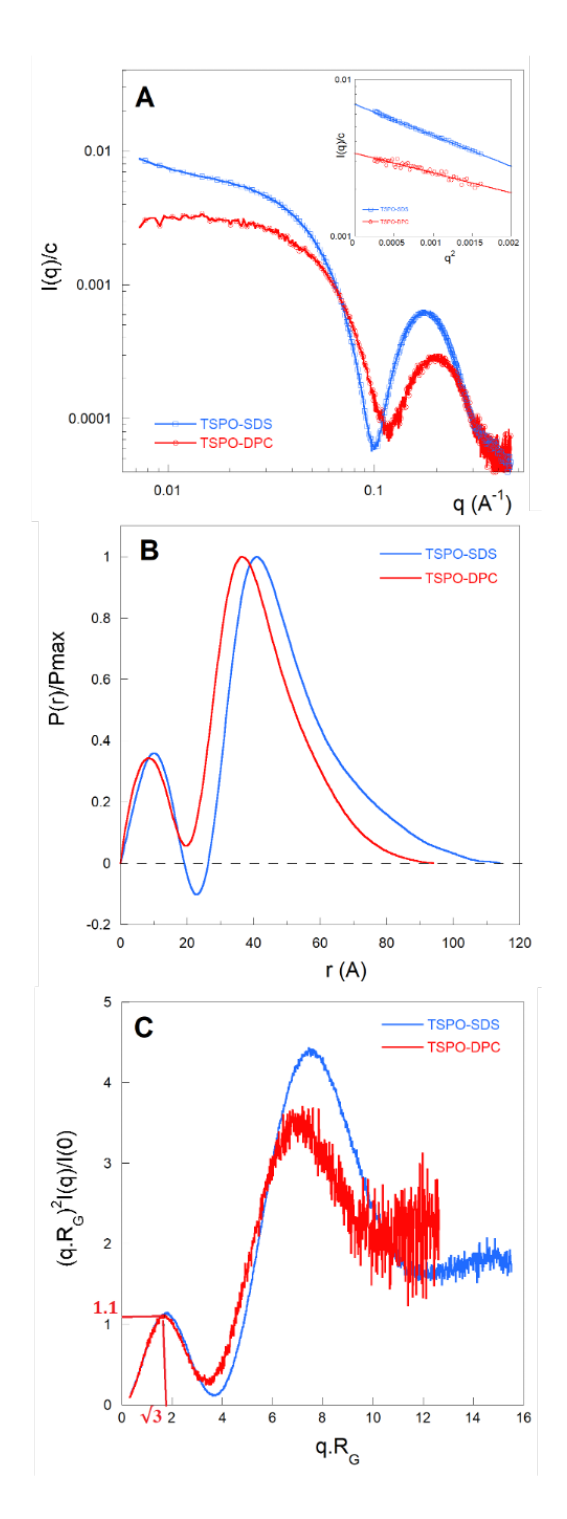


Figure 5. SEC-SAXS analysis of mTSPO-SDS (blue) and mTSPO-DPC (red). (\boldsymbol{A}) "Ideal" form factor (see 2.7 paragraph for details) and Guinier plots in insert, (\boldsymbol{B}) normalized pair-distance distribution function, and (\boldsymbol{C}) R_G -dimensionless Kratky plot.

Table 1. MALLS, SAXS, and SANS analysis of mTSPO in SDS or DPC environments.

	mTSPO-SDS	mTSPO-DPC
SEC-MALLS		
Protein molar mass (kDa)	19.0 ± 0.4	21.1 ± 0.2
Bound detergent molar molar mass (kDa)	39 ± 2	34.3 ± 0.7
Number of bound detergent molecules (N _{det})	135 ± 5	98 ± 2
SEC-SAXS		
mTSPO/detergent complex Guinier R_G (Å)	36.7 ± 0.1	30.5 ± 0.4
mTSPO/detergent R_{G} _GNOM (Å)	35.8 ± 0.05	29.9 ± 0.1
mTSPO/detergent $D_{max}(\text{Å})$	115 ± 5	95 ± 2
SEC-SANS		
mTSPO/h-detergent complex Guinier R_G (Å) (in 100% D ₂ O buffer)	25.41 ± 0.08	30.34 ± 0.06
d-detergent belt Guinier $R_G(\text{Å})$ (in 42% D ₂ O buffer)	25.3 ± 0.3	28.0 ± 0.8
mTSPO Guinier $R_G(\text{Å})$ (with d-detergent, in 100% D ₂ O buffer)	32 ± 2	24.7 ± 0.5
mTSPO R_{G} _GNOM (Å)	33.2 ± 0.3	24.61 ± 0.09
mTSPO $D_{max}(\text{Å})$	115 ± 3	77 ± 2

 R_G is determined from Guinier approximation in the reciprocal space (BioXTAS RAW software for SAXS analysis and NIST programs for SANS analysis). Parameters in the real space are calculated from GNOM (ATSAS package [20]).

As for mTSPO-SDS, three amounts (125, 250, 500 µg) of mTSPO-DPC were injected on the S75i column. From the three SAXS curves of mTSPO-DPC obtained from Foxtrot and BioXTAS RAW analysis, slightly attractive interaction effects could be observed both on forward intensity I(0) and radius of gyration R_G (Fig. S3). The radius of gyration (Fig. S3B) and I(0) (Fig. S3D) slightly increase with increasing amount of injected mTSPO, while the form of the mTSPO-DPC complex remains unchanged (the three concentration-normalized curves superimpose at q > 0.035 Å⁻¹). The form factor, the P(r) representation, and the dimensionless Kratky plot of mTSPO-DPC are superimposed with curves of mTSPO-SDS in Fig. 5. From the Guinier and the P(r) plots, R_G and D_{max} equal to 30.5 Å (Fig 5A, insert) and 95 Å, respectively. The mTSPO-DPC complex appears smaller than mTSPO-SDS complex as free DPC micelles are also smaller than free SDS micelles, as seing from SAXS analysis ($D_{max} \sim 57$ Å for DPC micelles, whereas $D_{max} \sim 75$ Å for SDS ones) (Pozza

& Bonneté, DIB). This can be correlated with SEC-MALLS data, showing that mTSPO binds fewer DPC than SDS molecules. Nevertheless, one can wonder if the difference in size between the two complexes are only due to a larger belt in SDS or a restructuration of the mTSPO-SDS complex. By comparing the P(r) of mTSPO-detergent complexes and free detergent micelles (Fig. S3, E-F), it appears that the maximum dimension of mTSPO-detergent complex is larger for SDS than for DPC, the difference between free micelles and mTSPO-detergent complexes being roughly the same (~ 40 Å), suggesting that the difference is only due to the presence of mTSPO. However, the positions on the abscissa of the two maxima and the minimum are slightly shifted to larger r values in SDS, indicating that mTSPO-detergent complex is different in shape. Moreover, the amplitude of the minimum in the case of SDS is more pronounced (even negative as for SDS micelles) than for DPC (which is positive compared to free DPC micelles). This means that the density core-contrast is decreased in DPC by the contribution of mTSPO electron density, probably due to a more compact protein structure in DPC than in SDS.

3.5.2. MemProt hybrid modeling of mTSPO detergent belt

In order to describe and compare mTSPO-detergent complexes in the two detergents and evaluate a belt model around mTSPO for each detergent, the SAXS curves of mTSPO-SDS and mTSPO-DPC (Fig. 5A) were fitted using the MemProt software [27] (Fig. S5). This program makes it possible to model a detergent corona with a collection of beads (representing dummy atoms) around the transmembrane domain of a membrane protein, using a known high-resolution structure (PDB file) of this protein. For the present study, we used, either the only known 3D-structure of mTSPO from NMR in presence of the ligand PK 11195 (2MGY.PDB), or the best AlphaFold model we found (Fig. S4). This corona is described as a hydrophobic layer of dimensions a and b and an outer hydrophilic layer of thickness t (see scheme p. 8 in SI). These parameters, as well as the ellipticity factor e of the corona, can vary in a range of values (defined by users, see [27]). To achieve the detergent-corona modeling, the electron densities (noted ρ in e/\tilde{A}^3) of the detergent head and tail have

to be determined in the buffer used for SAXS experiments to be implemented as parameters in MemProt, as well as the number of electrons in detergent head and tail. Since SDS is an ionic detergent, the buffer composition can influence the hydration of SDS head and therefore modifies the electron density values calculated from their chemical structures (Table S1). The electron densities of polar head and hydrophobic tail for each detergent were obtained by fitting the SAXS curves for SDS and DPC micelles (Pozza & Bonneté, DIB) and SLD (scattering length density) are reported in Table S1. From MemProt fitting, the electron density of the SDS hydrophobic core is $\rho = 0.260 \text{ e/Å}^3$, in agreement with the value obtained from SDS micelle fitting (Pozza & Bonneté, DIB). For the SDS hydrophilic head, the fitted electron density from MemProt $\rho = 0.397 \text{ e/Å}^3$ is clearly not in agreement with the value from SDS micelle model, $\rho = 0.471 \text{ e/Å}^3$. This can be due to the fact that the detergent packing in the micelle may be not exactly the same as around the protein. For the DPC hydrophilic head, the fitted electron density $\rho = 0.400 \text{ e/Å}^3$ is quite in good agreement with the value from DPC micelle model, $\rho = 0.387 \text{ e/Å}^3$.

MemProt molecular modeling shows a good agreement between the fit and the experimental data for SDS, a bit less good for DPC, using the 2MGY.PDB structure (Fig. S5A), while the fit is better using the AlphaFold model for DPC than for SDS (Fig. S5, D-E). However, this does not give consistent results for the number of bound detergents, the numbers of detergent head and tail being different in both cases (Tables S2-S3). Moreover, we found different numbers of bound detergent to mTSPO compared to the value determined by SEC-MALLS. We assumed that the disagreement in MemProt modeling is more probably due to the 3D-structure used for the protein (2MGY.PDB), which is the NMR structure of mTSPO in DPC but in presence of a stabilizing ligand (PK 11195) that stiffens the protein. However, the MemProt modeling using the AlphaFold model of His-tagged mTSPO, although giving better results in DPC, is also incorrect. The 3D-structure of mTSPO is therefore very probably less compact and/or even partially destabilized or unfolded in the conditions of the present study, as suggested by CD, fluorescence, and NMR studies (Figs. 1-3). Therefore, to

model mTSPO solution structure in SDS and in DPC, we used the contrast-matching technique in SEC-SANS to specifically probe the protein with a stealth detergent corona.

3.6. SEC-SANS analysis of mTSPO-detergent complex

3.6.1. Characterization of mTSPO-SDS complex by SEC-SANS

mTSPO-SDS samples were measured by SEC-SANS in different contrast-matching conditions to probe separately the whole complex as in SAXS (using hydrogenated SDS in 100% D₂O buffer), the detergent belt (using deuterated d-SDS in 42% D₂O buffer, that contrast-matches the protein), and the protein itself (using d-SDS in 100% D₂O buffer, that contrast-matches the detergent) (Fig. 6A).

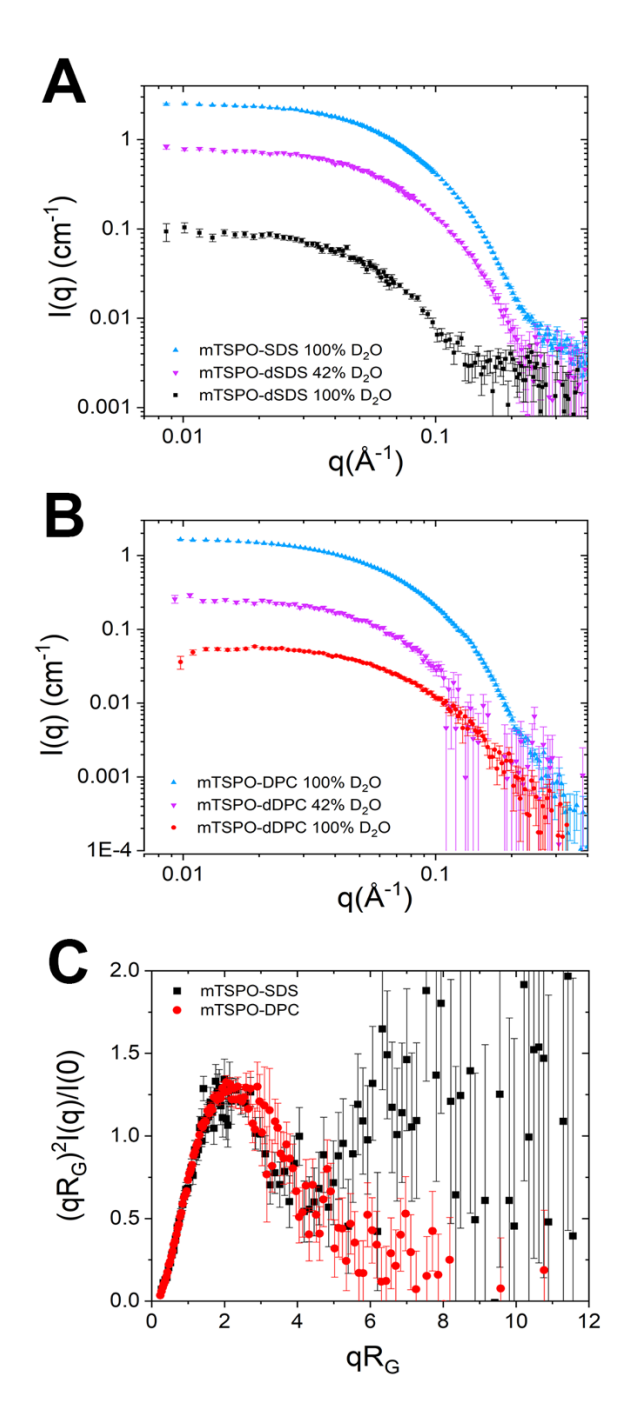


Figure 6. SEC-SANS curves in (*A*) SDS or (*B*) DPC detergent, probing mTSPO-detergent whole complex (mTSPO with hydrogenated detergent in 100% D_2O buffer, blue up triangles), detergent corona (mTSPO with deuterated d-detergent in 42% D_2O , purple down triangles), and mTSPO protein itself (mTSPO with stealth d-SDS (black squares) or d-DPC (red circles), in 100% D_2O). (*C*) R_G -dimensionless Kratky plots of mTPSO with d-SDS (black squares) or d-DPC (red circles) in 100% D_2O buffer.

Taking into account the contrast values and a ratio of ~10 between I(0) for SDS belt and the protein (*i.e.* curves for mTSPO-dSDS in 42% and 100% D₂O buffer, respectively) (Fig. 6A, Table 1), the SDS corona volume (mTSPO-dSDS in 42% D₂O buffer) was roughly estimated to be composed of ~200 molecules, which is significantly different but of the order of magnitude of the number of molecules reported by SEC-MALLS, and with a R_G of about 25 Å (Table 1). Note that the protein concentration cannot be evaluated precisely since I(0) for the protein curve (mTSPO-dSDS in 100% D₂O buffer) corresponds to an average of measurements made at different concentrations along the SEC-SANS chromatogram. At the elution peak, mTSPO concentration was evaluated to be ~0.2 mg/mL in SDS, as measured by *in situ* absorbance on the SEC-SANS experiment.

The radius of gyration of the unliganded ("apo") mTSPO in SDS (mTSPO-dSDS in 100% D_2O buffer), measured by contrast matching the bound detergent corona, was found to be ~32 Å (Table 1). This is much larger than the expected R_G ~18 Å calculated from the NMR structure (2MGY.PDB) and that of the AlphaFold model R_G ~21 Å. Without any ligand and in SDS detergent, the protein may not be in a native 3D conformation. The dimensionless Kratky plot (Fig. 6C) shows that mTSPO presents a globular 3D-structure in SDS, but with a maximum at a bit higher than $q.R_G$ $\approx \sqrt{3}$ [24]. However, the protein is very flexible since the curve does not exhibit a complete "bell" shape falling to zero, characteristic for compact proteins, nor a fully unfolded structure since the curve does not show a "plateau" at high q-values. The pair-distance distribution function of the SANS curve of mTSPO in SDS gives a large $D_{max} \sim 115$ Å (Fig. 7B, Table 1) suggesting an elongated conformation of the protein in SDS, the detergent used to solubilize mTSPO from inclusion bodies.

The theoretical SANS curves, calculated from both the 2MGY.PDB and the AlphaFold model using CRYSON software [34], are very far from the experimental data measured in SDS (Fig. S6). *Ab initio* reconstruction was performed using DENFERT software [29,30] (Fig. 7A). The most probable model and the filtered envelope from a pool of 10 DENFERT reconstructions were found using SUPCOMB software [35] (Fig. 7C). The superimposition of this envelope with the AlphaFold model calculated from His-tagged mTSPO sequence (Fig. S4), shows a significantly larger

conformation for unliganded mTSPO (*i.e.* the "apo" form of the protein, without any ligand bound) in SDS compared to the AlphaFold model (Fig. 7C). The Porod volume calculated with PRIMUS software [20] and the volume estimated from DENFERT modeling give ~35,000 and ~66,500 Å³, respectively. These values are much larger than the expected volume (~25,679 Å³) calculated from mTSPO molecular mass and using a protein density of 1.35 g cm⁻³.

Ab initio modeling confirms the structural information suggested by the Kratky plot, *i.e.* demonstrates that mTSPO in SDS is partially unfolded and very flexible (Fig. 6C). The protein has therefore not a native-functional conformation in this detergent, as already expected from its secondary helical structure measured by CD in this condition (Fig. 1) [34,5]. Indeed, the 30% helicity of mTSPO in SDS is significantly lower than the expected value of about 50% (since ~100 residues over 189 are involved in the transmembrane helices). These results are consistent with the impossibility for mTSPO to bind ligands in SDS, as reported before by ITC [5].

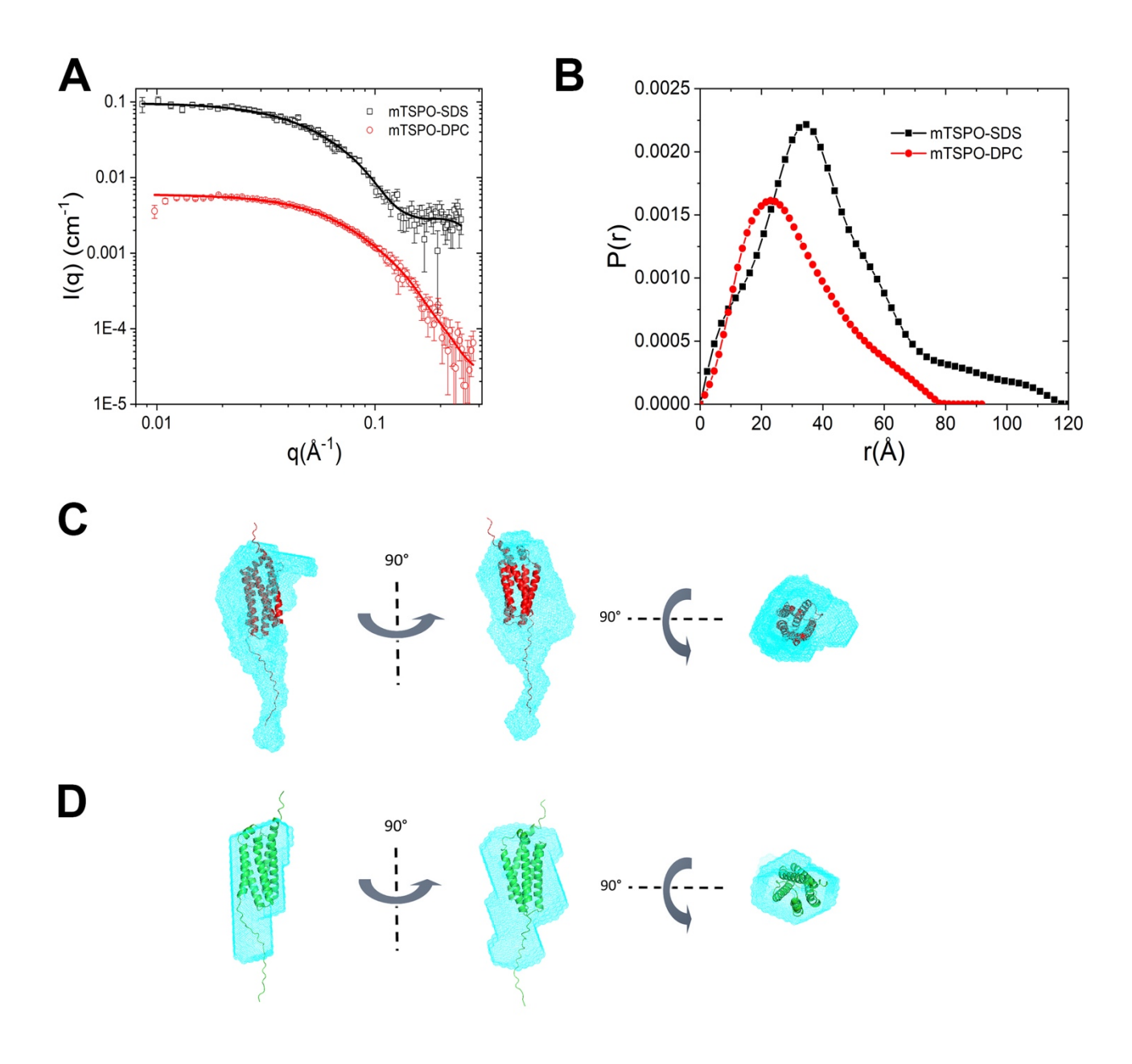


Figure 7. (A) SANS data of mTSPO obtained by measuring mTSPO-detergent complexes in 100 % D₂O buffer that contrast-matches the deuterated detergent (selected data from Fig. 6, A-B) and ab initio modeling using DENFERT software, in SDS (black squares and line) or DPC (red circles and line). (B) Pair-distance distribution functions of mTSPO in both conditions, showing a more elongated protein conformation in SDS (black squares) compared to DPC (red circles). Difference views of ab initio most probable envelopes (light blue) of mTSPO from a pool of 10 DENFERT reconstructions in (C) SDS or (D) DPC. The most precise AlphaFold model calculated from mTSPO His-tag sequence (Fig. S4) is superimposed in red or green, respectively. The envelopes and the

models are represented at the same scale. The SLD values used to fit the SANS data are listed in Table S1 (SI).

3.6.2. Characterization of mTSPO-DPC complex by SEC-SANS

Taking into account the contrast values and a ratio of \sim 5 between I(0) for DPC belt and the protein (*i.e.* curves for mTSPO-dDPC in 42% and 100% D₂O buffer, respectively) (Fig. 6B), the DPC corona was estimated to be composed of \sim 89 molecules, with a R_G of about 28 Å (Table 1), which is consistent with the value found by SEC-MALLS. The protein concentration was evaluated to be \sim 0.6 mg/mL at the elution peak in the SEC-SANS chromogram in DPC condition.

The radius of gyration of the unliganded mTSPO in DPC, measured by contrast matching the bound detergent (Figs. 6B and 7A), was found to be ~24.7 Å (Table 1), lower than R_G found in SDS (32 Å), but still larger than both the expected R_G ~18 Å calculated from the NMR structure (2MGY.PDB) in presence of PK 11195 and R_G ~21 Å estimated for the AlphaFold model. However, mTSPO is more compact in DPC than in SDS, as shown in the dimensionless Kratky representation (Fig. 6C) by the characteristic "bell" shape of the curve with the maximum observed not far from $q.R_G \approx \sqrt{3}$ [24]. The pair-distance distribution function P(r) of mTSPO in DPC gives a D_{max} value of ~77 Å, lower than the value found in SDS (115 Å) but slightly larger than the D_{max} from 2MGY.PDB structure obtained in DPC with the PK 11195 ligand (~67 Å) (Fig. 7B, Table 1), confirming a more compact conformation of the protein in DPC compared to SDS. This more "native" structuration is consistent with both higher helix content and inter-helical interactions (Fig. 3), as well as higher Trp fluorescence (Fig. 1), in DPC compared to SDS.

The theoretical SANS curves calculated using CRYSON software [20] from, either the liganded mTSPO in DPC (2MGY.PDB), or the AlphaFold model, are however still far from the experimental data (Fig. S6), suggesting that, without ligand, the protein remains in a more flexible and disordered state. *Ab initio* reconstruction from the SANS curve of mTSPO was performed using DENFERT software [29,30] (Fig. 7A). The most probable model and the filtered envelope from a

pool of 10 DENFERT reconstructions were found using SUPCOMB software [31] (Fig. 7D). The superimposition of this envelope with the most precise AlphaFold model obtained from His-tagged mTSPO sequence (Fig. S4), shows a closer but still larger conformation for the unliganded mTSPO in DPC (Fig. 7D), compared to the protein in SDS (Fig. 7C). In the present study without ligand, mTSPO is very flexible, especially its N-terminus (tag of 20 His residues) and C-terminus (flexible loop) parts. The SANS envelope gives therefore the average of several conformations the protein adopts in solution.

The Porod volumes calculated with PRIMUS (from ATSAS package) and estimated from DENFERT modeling give ~45,000 and ~59,400 ų, respectively, which is much larger than the expected volume (~25,679 ų) calculated from mTSPO molecular weight, using a density of 1.35 g cm⁻³. This may be attributed to the protein flexibility and partial unfolding in absence of a stabilizing ligand.

These volumes are roughly similar in both SDS and DPC, even though the protein exhibits a much more extended or even "unfolded" 3D-envelope in SDS. An unchanged volume together with a more extended conformation in SDS might be attributed to the opening of one or several helices from the transmembrane α -helix bundle, as reported before for a peripheric membrane protein [37]. Such an assumption would be consistent with the result that mTSPO still exhibits a helical secondary structure in SDS even if lower compared to DPC (Fig. 1). This is also in agreement with a protein "cavity" observed inside mTSPO by DENFERT modeling that may bind SDS molecules (Fig. S7), in agreement with the higher number of SDS molecules bound to mTSPO than DPC one, as measured by SEC-MALLS (Fig. 4).

The unliganded mTSPO protein conformation in DPC is significantly different from the PK 11195-binding mTSPO, the ligand stiffening the protein [7]. This is in agreement with a previous NMR study reporting that DPC is a detergent able to destabilize the structure of mTSPO [38]. Moreover, multiconformers of mTSPO have been reported in DPC in absence of ligand, that can lead to SANS polydispersity [7]. In contrast, the two bacterial TSPO crystallographic structures show a

strong similarity with and without ligand [6] and are clearly different from the NMR structure of mTSPO with PK 11195 ligand [39]. Therefore, one can wonder whether these structural differences are due, either to the bacterial or mammalian origin of TSPO, or to the use of different detergents depending on the techniques, as suggested by Guo *et al.* [12]. These observations may explain why no crystallographic structure has yet been obtained with recombinant mammalian TSPO [5,7,39]. The choice of the detergent is known to be a crucial step to stabilize membrane proteins [38] and maintain them in a native folding [40,41], especially membrane proteins in α -helices. Hence, in liposomes, mTSPO is stabilized but only in monomers and using both cholesterol and a stabilizing ligand [42], confirming that mTSPO, as shown by solid state NMR, is instable in liposomes except in presence of ligand [43]. As well, long chain lipids or lipid mixture can stabilize mTSPO but not better than DMPC lipid and the presence of the ligand remains essential [44].

The present study highlights the difficulty in stabilizing the conformation of a transmembrane protein, depending on the detergent or lipid environment. Its characterization is also dependent upon the techniques and the softwares available for analysis and modeling. We show for the first time, by combining SEC-SANS and DENFERT modeling, the effect of the detergent environment on the solution structure of mTSPO. Further investigation is needed to determine mTSPO conformation in a more biomimetic environment with a mixture of lipid/detergent or only lipids [8], in which mTSPO "activity" (*i.e.* affinity for ligands) would be the highest one [9].

4. CONCLUSIONS

We report here the influence of the amphiphilic environment on the solution structure of the mouse mTSPO, combining optical spectroscopy, SEC-MALLS, SEC-SAS, and molecular modeling. Using SANS and the contrast matching technique, which makes the detergent corona stealth, we show that mTSPO conformation is more flexible, partially misfolded, and more elongated in SDS, consistently with the lower helicity content reported in this detergent. The change of environment by replacing SDS by DPC improves significantly mTSPO folding and compaction, in agreement with higher helicity content and helical interactions, as measured by CD. DPC detergent changes also the structural local environment of the 12 Trp residues of mTSPO, as observed by the strong increase in intrinsic fluorescence. However, the 3D solution structure of the ligand-free mTSPO in DPC remains significantly different compared to the NMR structure obtained in DPC but in presence of a stabilizing ligand. Likewise, 1D 1H NMR spectra show a still incomplete spreading of the protein Trp indoles.

DECLARATION OF INTEREST

The authors declare no competing interests.

AUTHOR CONTRIBUTIONS

SC, FB, SF, and JJL designed research; all co-authors conducted and/or performed experiments; SC, FB, SF, AK, and JJL analyzed data; SC, FB, and JJL wrote the paper.

AKNOWLEDGMENTS

This work was financially supported by the CNRS (MITI 2021 and Tremplin@INP 2021). We gratefully acknowledge ESRF, SOLEIL, and ILL large-scale facilities for beamtime on BM29, SWING, and D22 beamlines, respectively, and we thank Dr Petra Pernot (BM29), Dr Aurélien Thureau (SWING) and Dr Lionel Porcar (D22) for their assistance. We thank also Dr Martina Sandroni, as responsible of ILL Chemistry Lab, for technical assistance in sample preparation, as well as Zaynab Alsalman and Soukaina Boutchkalt for their help in the framework of their Master internships. We are very grateful to Dr Pierre Legrand (PROXIMA-1 beamline, SOLEIL) for the calculation of the AlphaFold models of His6-tagged mTSPO. This work benefited from the use of the SasView application, originally developed under NSF award DMR-0520547. SasView contains code developed with funding from the European Union's Horizon 2020 research and innovation program under the SINE2020 project, grant agreement No 654000.

REFERENCES

- [1] V. Papadopoulos, M. Baraldi, T.R. Guilarte, T.B. Knudsen, J.J. Lacapère, P. Lindemann, M.D. Norenberg, D. Nutt, A. Weizman, M.R. Zhang, M. Gavish, Translocator protein (18 kDa): new nomenclature for the peripheral-type benzodiazepine receptor based on its structure and molecular function, Trends Pharmacol. Sci. 27 (2006) 402–409. https://doi.org/10.1016/j.tips.2006.06.005.
- [2] O.M. Downer, R.E.G. Marcus, N.R. Zürcher, J.M. Hooker, Tracing the History of the Human Translocator Protein to Recent Neurodegenerative and Psychiatric Imaging, ACS Chem. Neurosci. 11 (2020) 2192–2200. https://doi.org/10.1021/acschemneuro.0c00362.
- [3] J.J. Lacapere, L. Duma, S. Finet, M. Kassiou, V. Papadopoulos, Insight into the Structural Features of TSPO: Implications for Drug Development, Trends Pharmacol. Sci. 41 (2020) 110–122. https://doi.org/10.1016/j.tips.2019.11.005.
- [4] A. Bruno, E. Barresi, N. Simola, E. Da Pozzo, B. Costa, E. Novellino, F. Da Settimo, C. Martini, S. Taliani, S. Cosconati, Unbinding of Translocator Protein 18 kDa (TSPO)
 Ligands: From in Vitro Residence Time to in Vivo Efficacy via in Silico Simulations, ACS
 Chem. Neurosci. 10 (2019) 3805–3814. https://doi.org/10.1021/acschemneuro.9b00300.
- [5] J.J. Lacapere, Structural studies of TSPO, a mitochondrial membrane protein, in: Membr. Proteins Prod. Struct. Anal., Springer Science Business Media New York, 2014: pp. 393–421. https://doi.org/10.1007/978-1-4939-0662-8 14.
- [6] Y. Guo, R.C. Kalathur, Q. Liu, B. Kloss, R. Bruni, C. Ginter, E. Kloppmann, B. Rost, W.A. Hendrickson, Structure and activity of tryptophan-rich TSPO proteins, Science (80-.). 347 (2015) 551–555. https://doi.org/10.1126/science.aaa1534.
- [7] Ł. Jaremko, M. Jaremko, K. Giller, S. Becker, M. Zweckstetter, Conformational Flexibility in the Transmembrane Protein TSPO, Chem. A Eur. J. 21 (2015) 16555–16563. https://doi.org/10.1002/chem.201502314.
- [8] J.J. Lacapère, F. Delavoie, H. Li, G. Péranzi, J. Maccario, V. Papadopoulos, B. Vidic,

- Structural and functional study of reconstituted peripheral benzodiazepine receptor, Biochem. Biophys. Res. Commun. 284 (2001) 536–541. https://doi.org/10.1006/bbrc.2001.4975.
- [9] S. Iatmanen-Harbi, L. Senicourt, V. Papadopoulos, O. Lequin, J.J. Lacapere, Characterization of the high-affinity drug ligand binding site of mouse recombinant TSPO, Int. J. Mol. Sci. 20 (2019). https://doi.org/10.3390/ijms20061444.
- [10] L. Jaremko, M. Jaremko, K. Giller, S. Becker, M. Zweckstetter, Structure of the Mitochondrial Translocator Protein in Complex with a Diagnostic Ligand, Science (80-.). 1363 (2014) 1363–1367. https://doi.org/DOI: 10.1126/science.1248725.
- [11] F. Li, J. Liu, R.M. Garavito, S. Ferguson-Miller, Evolving understanding of translocator protein 18 kDa (TSPO), Pharmacol. Res. 99 (2015) 404–409.
 https://doi.org/10.1016/j.phrs.2015.03.022.
- [12] Y. Guo, Be Cautious with Crystal Structures of Membrane, Crystals. 10 (2020) 86.
- [13] L. Senicourt, S. Iatmanen-Harbi, C. Hattab, M.A. Ostuni, M.-F. Giraud, J.J. Lacapère, Recombinant overexpression of mammalian TSPO isoforms 1 and 2, in: Membr. Protein Struct. Funtion Charact., Springer, 2017: pp. 1–25. https://doi.org/10.1007/978-1-4939-7151-0 1.
- [14] S. Mehboob, B.H. Luo, B.M. Patel, L.W. Fung, alpha beta Spectrin coiled coil association at the tetramerization site, Biochemistry. 40 (2001) 12457–12464. http://www.ncbi.nlm.nih.gov/pubmed/11591167.
- [15] S. Legardinier, C. Raguénès-Nicol, C. Tascon, C. Rocher, S. Hardy, J.F. Hubert, E. Le Rumeur, Mapping of the Lipid-Binding and Stability Properties of the Central Rod Domain of Human Dystrophin, J. Mol. Biol. 389 (2009) 546–558.

 https://doi.org/10.1016/j.jmb.2009.04.025.
- [16] A. Micsonai, F. Wien, É. Bulyáki, J. Kun, É. Moussong, Y.H. Lee, Y. Goto, M. Réfrégiers, J. Kardos, BeStSel: A web server for accurate protein secondary structure prediction and fold

- recognition from the circular dichroism spectra, Nucleic Acids Res. 46 (2018) W315–W322. https://doi.org/10.1093/nar/gky497.
- [17] K. Gimpl, J. Klement, S. Keller, Characterising protein/detergent complexes by triple-detection size-exclusion chromatography, Biol. Proced. Online. 18 (2016) 1–18. https://doi.org/10.1186/s12575-015-0031-9.
- [18] A. Thureau, P. Roblin, J. Pérez, BioSAXS on the SWING beamline at Synchrotron SOLEIL,
 J. Appl. Crystallogr. 54 (2021) 1698–1710. https://doi.org/10.1107/s1600576721008736.
- [19] S. Combet, An introduction to neutrons for biology, in: S. Combet, G. Schiro (Eds.), EPJ Web of, 2020. https://doi.org/10.1051/epjconf/202023601001.
- [20] K. Manalastas-Cantos, P. V. Konarev, N.R. Hajizadeh, A.G. Kikhney, M. V. Petoukhov, D.S. Molodenskiy, A. Panjkovich, H.D.T. Mertens, A. Gruzinov, C. Borges, C.M. Jeffries, D.I. Sverguna, D. Frankea, ATSAS 3.0: Expanded functionality and new tools for small-angle scattering data analysis, J. Appl. Crystallogr. 54 (2021) 343–355. https://doi.org/10.1107/S1600576720013412.
- [21] C.D. Putnam, M. Hammel, G.L. Hura, J.A. Tainer, X-ray solution scattering (SAXS) combined with crystallography and computation: Defining accurate macromolecular structures, conformations and assemblies in solution, Q. Rev. Biophys. 40 (2007) 191–285. https://doi.org/10.1017/S0033583507004635.
- [22] E. Walenta, Small angle x-ray scattering. Von O. GLATTER und O. KRATKY. London: Academic Press Inc. Ltd. 1982. ISBN 0-12-286280-5. X, 515 Seiten, geb. £ 43,60; US
 \$ 81.00, Acta Polym. 36 (1985) 296. https://doi.org/10.1002/actp.1985.010360520.
- [23] V. Receveur-Brechot, D. Durand, How Random are Intrinsically Disordered Proteins? A Small Angle Scattering Perspective, Curr. Protein Pept. Sci. 13 (2012) 55–75. https://doi.org/10.2174/138920312799277901.
- [24] V.M. Burger, D.J. Arenas, C.M. Stultz, A Structure-free Method for Quantifying Conformational Flexibility in proteins, Sci. Rep. 6 (2016) 1–9.

- https://doi.org/10.1038/srep29040.
- [25] J.B. Hopkins, R.E. Gillilan, S. Skou, BioXTAS RAW: Improvements to a free open-source program for small-angle X-ray scattering data reduction and analysis, J. Appl. Crystallogr. 50 (2017) 1545–1553. https://doi.org/10.1107/S1600576717011438.
- [26] N.T. Johansen, M.C. Pedersen, L. Porcar, A. Martel, L. Arleth, Introducing SEC-SANS for studies of complex self-organized biological systems, Acta Crystallogr. Sect. D Struct. Biol. 74 (2018) 1178–1191. https://doi.org/10.1107/S2059798318007180.
- [27] J. Pérez, A. Koutsioubas, Memprot: A program to model the detergent corona around a membrane protein based on SEC-SAXS data, Acta Crystallogr. Sect. D Biol. Crystallogr. 71 (2015) 86–93. https://doi.org/10.1107/S1399004714016678.
- [28] A. Berthaud, J. Manzi, J. Pérez, S. Mangenot, Modeling detergent organization around aquaporin-0 using small-angle X-ray scattering, J. Am. Chem. Soc. 134 (2012) 10080–10088. https://doi.org/10.1021/ja301667n.
- [29] A. Koutsioubas, S. Jaksch, J. Pérez, DENFERT version 2: Extension of ab initio structural modelling of hydrated biomolecules to the case of small-angle neutron scattering data, J. Appl. Crystallogr. 49 (2016) 690–695. https://doi.org/10.1107/S1600576716003393.
- [30] A. Koutsioubas, J. Pérez, Incorporation of a hydration layer in the "dummy atom" ab initio structural modelling of biological macromolecules, J. Appl. Crystallogr. 46 (2013) 1884–1888. https://doi.org/10.1107/S0021889813025387.
- [31] D. Franke, M. V. Petoukhov, P. V. Konarev, A. Panjkovich, A. Tuukkanen, H.D.T. Mertens, A.G. Kikhney, N.R. Hajizadeh, J.M. Franklin, C.M. Jeffries, D.I. Svergun, ATSAS 2.8: A comprehensive data analysis suite for small-angle scattering from macromolecular solutions, J. Appl. Crystallogr. 50 (2017) 1212–1225. https://doi.org/10.1107/S1600576717007786.
- [32] M. Mirdita, K. Schütze, Y. Moriwaki, L. Heo, S. Ovchinnikov, M. Steinegger, ColabFold: making protein folding accessible to all, Nat. Methods. 19 (2022). https://doi.org/10.1038/s41592-022-01488-1.

- [33] J. Jumper, R. Evans, A. Pritzel, T. Green, M. Figurnov, O. Ronneberger, K. Tunyasuvunakool, R. Bates, A. Žídek, A. Potapenko, A. Bridgland, C. Meyer, S.A.A. Kohl, A.J. Ballard, A. Cowie, B. Romera-Paredes, S. Nikolov, R. Jain, J. Adler, T. Back, S. Petersen, D. Reiman, E. Clancy, M. Zielinski, M. Steinegger, M. Pacholska, T. Berghammer, S. Bodenstein, D. Silver, O. Vinyals, A.W. Senior, K. Kavukcuoglu, P. Kohli, D. Hassabis, Highly accurate protein structure prediction with AlphaFold, Nature. 596 (2021) 583–589. https://doi.org/10.1038/s41586-021-03819-2.
- [34] D.I. Svergun, S. Richard, M.H.J. Koch, Z. Sayers, S. Kuprin, G. Zaccai, Protein hydration in solution: Experimental observation by x-ray and neutron scattering, Proc. Nat. Acad. Sci. USA. 95 (1998) 2267–2272. https://doi.org/10.1073/pnas.95.5.2267.
- [35] V. V. Volkov, D.I. Svergun, Uniqueness of ab initio shape determination in small-angle scattering, J. Appl. Crystallogr. 36 (2003) 860–864.
 https://doi.org/10.1107/S0021889803000268.
- [36] S. Murail, J.-C. Robert, Y.M. Coïc, J.-M. Neumann, M.A. Ostuni, Z.X. Yao, V. Papadopoulos, N. Jamin, J.-J. Lacapère, Secondary and tertiary structures of the transmembrane domains of the translocator protein TSPO determined by NMR. Stabilization of the TSPO tertiary fold upon ligand binding, Biochim. Biophys. Acta Biomembr. 1778 (2008) 1375–1381. https://doi.org/10.1016/j.bbamem.2008.03.012.
- [37] R. Dos Santos Morais, O. Delalande, J. Pérez, D. Mias-Lucquin, M. Lagarrigue, A. Martel, A.-E. Molza, A. Chéron, C. Raguénès-Nicol, T. Chenuel, A. Bondon, M.-S. Appavou, E. Le Rumeur, S. Combet, J.-F. Hubert, Human Dystrophin Structural Changes upon Binding to Anionic Membrane Lipids, Biophys. J. 115 (2018) 1231–1239. https://doi.org/10.1016/j.bpj.2018.07.039.
- [38] Y. Xia, K. Ledwitch, G. Kuenze, A. Duran, J. Li, C.R. Sanders, C. Manning, J. Meiler, A unified structural model of the mammalian translocator protein (TSPO), J. Biomol. NMR. 73 (2019) 347–364. https://doi.org/10.1007/s10858-019-00257-1.

- [39] F. Li, J. Liu, N. Liu, L.A. Kuhn, R.M. Garavito, S. Ferguson-Miller, Translocator Protein 18 kDa (TSPO): An Old Protein with New Functions?, Biochemistry. 55 (2016) 2821–2831. https://doi.org/10.1021/acs.biochem.6b00142.
- [40] M. Zoonens, J. Comer, S. Masscheleyn, E. Pebay-Peyroula, C. Chipot, B. Miroux, F. Dehez, Dangerous Liaisons between detergents and membrane proteins. the case of mitochondrial uncoupling protein 2, J. Am. Chem. Soc. 135 (2013) 15174–15182. https://doi.org/10.1021/ja407424v.
- [41] V. Kurauskas, A. Hessel, P. Ma, P. Lunetti, K. Weinhäupl, L. Imbert, B. Brutscher, M.S. King, R. Sounier, V. Dolce, E.R.S. Kunji, L. Capobianco, C. Chipot, F. Dehez, B. Bersch, P. Schanda, How Detergent Impacts Membrane Proteins: Atomic-Level Views of Mitochondrial Carriers in Dodecylphosphocholine, J. Phys. Chem. Lett. 9 (2018) 933–938. https://doi.org/10.1021/acs.jpclett.8b00269.
- [42] G. Jaipuria, A. Leonov, K. Giller, S.K. Vasa, Á. Jaremko, M. Jaremko, R. Linser, S. Becker, M. Zweckstetter, Cholesterol-mediated allosteric regulation of the mitochondrial translocator protein structure, Nat. Commun. 8 (2017) 1–8. https://doi.org/10.1038/ncomms14893.
- [43] L. Duma, L. Senicourt, B. Rigaud, V. Papadopoulos, J.J. Lacapère, Solid-state NMR study of structural heterogeneity of the apo WT mouse TSPO reconstituted in liposomes, Biochimie. (2022). https://doi.org/10.1016/j.biochi.2022.08.013.
- [44] G. Rivière, G. Jaipuria, L.B. Andreas, A. Leonov, K. Giller, S. Becker, M. Zweckstetter, Membrane-embedded TSPO: an NMR view, Eur. Biophys. J. 50 (2021) 173–180. https://doi.org/10.1007/s00249-020-01487-0.